THE UNIVERSITY OF ALBERTA

FINITE DEFORMATION OF A POLYURETHANE RUBBER IN COMPRESSION

BY

WILLIAM M.J. MAH

A THESIS

SUBMITTED TO THE FACULTY OF GRADUATE STUDIES AND RESEARCH

IN PARTIAL FULFILMENT OF THE REQUIREMENTS FOR THE DEGREE

OF MASTER OF SCIENCE

DEPARTMENT OF MECHANICAL ENGINEERING

EDMONTON, ALBERTA

SPRING, 1973

ABSTRACT

This thesis investigates the mechanical behavior of a hard polyurethane rubber in compression in the temperature range of 0°F to 70°F. A compression test is chosen because data on this type of deformation are lacking and the material is often used in compression. The neo-Hookean, Mooney and Ogden models are shown to be inadequate in predicting the elastic response of this material. A new model based on the Rivlin-Saunders form of the strain energy function is proposed. An attempt is made to model the viscoelastic behavior of this material with a simple nonlinear Kelvin-Voigt model. The effect of temperature on the elastic behavior is insignificant in the temperature range studied but the viscoelastic response appears to be affected.

ACKNOWLEDGMENT

The author wishes to thank Dr. J.B. Haddow for his patience and guidance in the supervision of this thesis. The assistance of the members of the Mechanical Engineering Shop during system modifications and sample preparation is greatly appreciated. Also, the graduate students who offered many helpful suggestions are not be forgotten. Miss H. Wozniuk is to be commended on her typing of this thesis.

TABLE OF CONTENTS

LIST OF FIGURES

LIST OF SYMBOLS

A	current cross-sectional area of the sample
A_0	initial undeformed cross-sectional area of the sample
$\underset{\sim}{B}$	Cauchy deformation tensor
$\underset{\sim}{C}$	Green deformation tensor
$\underset{\sim}{d}$	rate of deformation tensor
E	Young's modulus
$\underset{\sim}{F}$	deformation gradient tensor
$\underset{\sim}{I}$	unit tensor
k	spring constant
ℓ	current deformed length of the sample
ℓ_0	initial undeformed length of the sample
$\underset{\sim}{Q}$	a proper orthogonal tensor
$\underset{\sim}{R}$	a rotation tensor
t	time
$\underset{\sim}{U}$	a positive-definite symmetric deformation tensor
W	strain energy function

Greek letters

η	viscosity coefficient
λ	extension ratio
μ	classical shear modulus
$\underset{\sim}{\sigma}$	stress tensor

Superscripts

e	elastic component
T	transpose
v	viscous component
.	differentiation with respect to time

CHAPTER I

INTRODUCTION

The subject of this investigation is the determination of the mechanical behavior of a polyurethane rubber at various temperatures. The material is assumed to be homogeneous, isotropic, and incompressible and thus may be treated as a continuum. The theory of finite elasticity and viscoelasticity is used to develop a theoretical model for this material.

Previous investigators of rubber-like elasticity have used tension tests and shear tests to provide data. Since there is a lack in data from compression tests and also because the material under investigation is often used in compression, a compression test is to be used. Use of such a test will eliminate the stability problem of necking encountered in tension tests.

One of the problems involved in this investigation is the temperature control system. To determine if the material behavior is temperature dependent, the sample must be maintained at the test temperature within a tolerance of $\pm$ 2°F. Another problem arises from the nature of the compression test; that is, the friction between the platens of the subpress and the sample during a test, as shown in Figure 1(a).

The theoretical problem is to derive a model that will predict the response of the material. The material is assumed to be

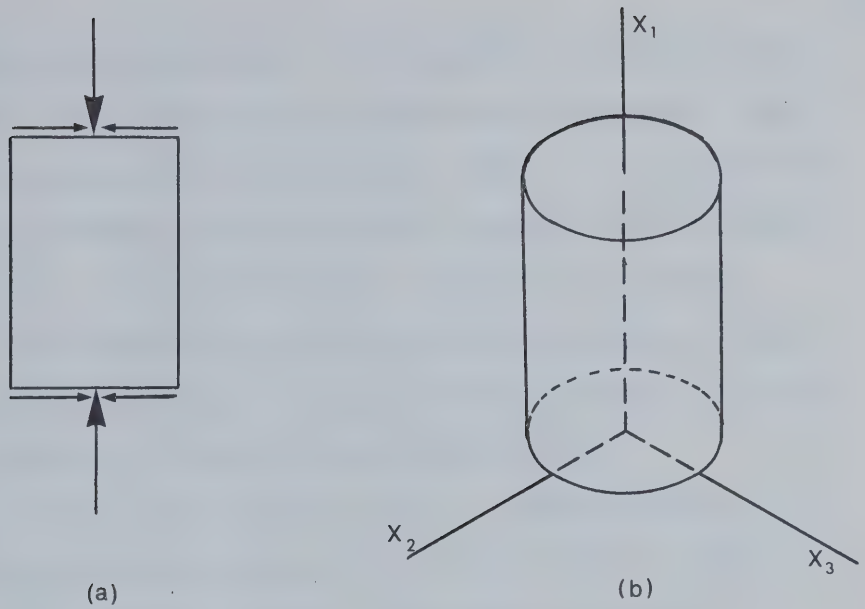

FIGURE 1 LOAD DIAGRAM AND COORDINATE SYSTEM

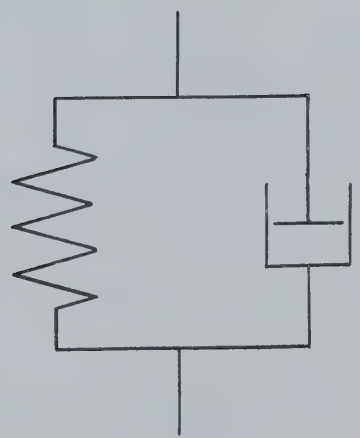

FIGURE 2 KELVIN-VOIGT MODEL

a nonlinear Kelvin-Voigt solid. If the samples are loaded as shown in Figure 1, it is assumed that a spring-dashpot combination, shown in Figure 2 may be used as the mechanical model. It is assumed that the spring represents the elastic part of the stress and the dashpot represents the viscous or dissipative component of the stress.

A rectangular Cartesian coordinate system shown in Figure 1(b) is chosen to facilitate the use of Cartesian tensors. The summation convention is followed unless otherwise noted.

The particular material studied is Vibrathane 6006, a polyester-based urethane elastomer, which has been cast to a hardness of 55 to 56 on the Shore D scale. The specimens are cured for 3 hours at 312°F and then 12 hours at 160-170°F. The oil resistant qualities of this material make it highly suitable for oil field service. In one application, the material is subjected to large compressive loads in temperature range of 0°F to 80°F.

CHAPTER II

THEORY

Assumptions

The material is assumed to be a homogeneous, isotropic, incompressible solid which may be modelled by the nonlinear Kelvin-Voigt mechanical model. The basic element of this model is a spring in parallel with a dashpot. With this assumption, the stress tensor may be decomposed into two parts: an elastic part and a viscous part. It is assumed that the elastic part may be derived using the methods of finite elasticity; the viscous part is derived from the theory of viscoelasticity. In the derivations of theoretical models, the effect of temperature is neglected.

The Elastic Component of Stress

The constitutive equation for a purely elastic solid, represented by a spring, may be derived mechanically without consideration of thermodynamic effects. The stress components are defined as single-valued functions of the deformation gradients:

$$\underset{\sim}{\sigma}^{(e)} = \underset{\sim}{f}(\underset{\sim}{F}) \qquad (1)$$

where $\underset{\sim}{\sigma}^{(e)}$ = the elastic stress tensor

$\underset{\sim}{f}$ = a tensor function

$\underset{\sim}{F}$ = the deformation gradient tensor

Since rigid body rotations do not affect the stress, the function, $\underset{\sim}{f}$, must satisfy

$$\underset{\sim}{Q}\ \underset{\sim}{f}(\underset{\sim}{F})\ \underset{\sim}{Q}^{T} = \underset{\sim}{f}(\underset{\sim}{Q}\underset{\sim}{F}) \tag{2}$$

where $\underset{\sim}{Q}$ is any proper orthogonal tensor. From polar decomposition

$$\underset{\sim}{F} = \underset{\sim}{R}\underset{\sim}{U} \tag{3}$$

uniquely; $\underset{\sim}{R}$ is a rotation tensor and $\underset{\sim}{U}$ is a positive-definite, symmetric deformation tensor. Thus equation (2) may be written

$$\underset{\sim}{f}(\underset{\sim}{F}) = \underset{\sim}{Q}^{T}\ \underset{\sim}{f}(\underset{\sim}{Q}\underset{\sim}{R}\underset{\sim}{U})\underset{\sim}{Q} \tag{4}$$

Now since $\underset{\sim}{R}^{T}$ is an orthogonal tensor, substitution of $\underset{\sim}{R}^{T}$ for $\underset{\sim}{Q}$ in equation (4) gives

$$\underset{\sim}{f}(\underset{\sim}{F}) = \underset{\sim}{R}\underset{\sim}{f}(\underset{\sim}{U})\underset{\sim}{R}^{T} \tag{5}$$

which shows $\underset{\sim}{f}$ to be a function of the six independent components of $\underset{\sim}{U}$. Also it may be shown that this is a necessary and sufficient condition for equation (2) to hold. Due to the difficulty in obtaining $\underset{\sim}{R}$ and $\underset{\sim}{U}$, let

$$\underset{\sim}{h}(\underset{\sim}{U}) = \underset{\sim}{U}^{-1}\underset{\sim}{f}(\underset{\sim}{U})\ \underset{\sim}{U}^{-1} \tag{6}$$

Then

$$\underset{\sim}{\sigma}^{(e)} = \underset{\sim}{F}\underset{\sim}{h}(\underset{\sim}{U})\ \underset{\sim}{F}^{T} \tag{7}$$

Introducing the Green deformation tensor, $\underset{\sim}{C} = \underset{\sim}{U}^2 = \underset{\sim}{F}^T\underset{\sim}{F}$,

$$\underset{\sim}{\phi}(\underset{\sim}{C}) = \underset{\sim}{h}(\underset{\sim}{U}) \tag{8}$$

and equation (5) becomes

$$\underset{\sim}{\sigma}^{(e)} = \underset{\sim}{F}\underset{\sim}{\phi}(\underset{\sim}{C})\ \underset{\sim}{F}^{T} \tag{9}$$

From the assumption of isotropy, $\underset{\sim}{\phi}$ must be an isotropic function of $\underset{\sim}{C}$:

$$\underset{\sim}{\phi} = \phi_0\underset{\sim}{I} + \phi_1\underset{\sim}{C} + \phi_2\underset{\sim}{C}^2 \tag{10}$$

where ϕ_0, ϕ_1, ϕ_2 are scalar functions of the scalar invariants of $\underset{\sim}{C}$ and $\underset{\sim}{I}$ is the unit tensor. The invariants are

$$\begin{aligned} I_1 &= \text{tr}\ \underset{\sim}{C}\ , \\ I_2 &= \tfrac{1}{2}\left[(\text{tr}\ \underset{\sim}{C})^2 - \text{tr}\ \underset{\sim}{C}^2\right] \\ I_3 &= \det \underset{\sim}{C} \end{aligned} \tag{11}$$

Alternatively, the invariants and equation (10) may be expressed in terms of the Cauchy deformation tensor, $\underset{\sim}{B} = \underset{\sim}{F}\underset{\sim}{F}^T$, giving

$$\underset{\sim}{\sigma}^{(e)} = \phi_0\underset{\sim}{B} + \phi_1\underset{\sim}{B}^2 + \phi_2\underset{\sim}{B}^3 \tag{12}$$

Using the Cayley-Hamilton theorem,

$$\underset{\sim}{B}^3 - I_1\underset{\sim}{B}^2 + I_2\underset{\sim}{B} - I_3\underset{\sim}{I} = 0 \tag{13}$$

equation (12) becomes

$$\underset{\sim}{\sigma}^{(e)} = \psi_0\underset{\sim}{I} + \psi_1\underset{\sim}{B} + \psi_2\underset{\sim}{B}^2 \tag{14}$$

where the response functions ψ_0, ψ_1, ψ_2 are new functions of I_1, I_2, I_3. From the condition of incompressibility,

$$I_3 = 1 \tag{15}$$

equation (14) reduces to

$$\underset{\sim}{\sigma}^{(e)} = -p\underset{\sim}{I} + \psi_1\underset{\sim}{B} + \psi_2\underset{\sim}{B}^2 \tag{16}$$

where p is a Lagrangian multiplier representing a arbitrary hydrostatic pressure and ψ_1, ψ_2 are functions of I_1, I_2 only. Thus equation (16) is the constitutive equation for a homogeneous, isotropic, incompressible elastic solid.

The use of thermodynamic concepts results in a more restrictive form of equation (16). A strain energy function, which determines the mechanical properties of the material, is postulated. This function is equivalent to the free energy for isothermal deformations and to the internal energy for isentropic deformations. Assuming that the strain energy is a single-valued function of the deformation gradients:

$$W = W(\underset{\sim}{F}) \ , \tag{17}$$

an energy balance will yield

$$\underset{\sim}{\sigma}^{(e)} = - p\underset{\sim}{I} + 2\left(\frac{\partial W}{\partial I_1} + I_1 \frac{\partial W}{\partial I_2}\right)\underset{\sim}{B} - 2 \frac{\partial W}{\partial I_2} \underset{\sim}{B}^2 \tag{18}$$

Comparison of equation (18) with equation (16) shows that the response functions of equation (16) have the form

$$\begin{aligned} \psi_1 &= 2\left(\frac{\partial W}{\partial I_1} + I_1 \frac{\partial W}{\partial I_2}\right) \ , \\ \psi_2 &= - 2 \frac{\partial W}{\partial I_2} \end{aligned} \tag{19}$$

In Cartesian tensor notation equation (18) becomes

$$\sigma_{ij}^{(e)} = - p\delta_{ij} + 2\left(\frac{\partial W}{\partial I_1} + I_1 \frac{\partial W}{\partial I_2}\right)B_{ij} - 2 \frac{\partial W}{\partial I_2} B_{ik}B_{kj} \tag{20}$$

For simple uniaxial compression as shown in Figure 1, it

is assumed that the sample is free to expand radially and that no barrelling occurs. Let the deformation in the axial direction be λ, given by

$$\lambda = \frac{\ell}{\ell_0} \tag{21}$$

where ℓ is the deformed length of the cylindrical sample and ℓ_0 is the undeformed length. For the coordinate system shown in Figure 1(b), this corresponds to the principal extension ratio, λ_1. From the incompressibility condition,

$$\lambda_1\lambda_2\lambda_3 = 1 \tag{22}$$

the other extension ratios are

$$\lambda_2 = \lambda_3 = \frac{1}{\sqrt{\lambda}} \tag{23}$$

In terms of the extension ratio, the strain invariants are

$$\begin{aligned} I_1 &= \lambda_1^2 + \lambda_2^2 + \lambda_3^2 = \lambda^2 + \frac{2}{\lambda} \\ I_2 &= \lambda_1^2\lambda_2^2 + \lambda_2^2\lambda_3^2 + \lambda_3^2\lambda_1^2 = 2\lambda + \frac{1}{\lambda^2} \\ I_3 &= \lambda_1^2\lambda_2^2\lambda_3^2 = 1 \end{aligned} \tag{24}$$

The Cauchy deformation tensor is

$$\underset{\sim}{B} = \begin{bmatrix} \lambda^2 & 0 & 0 \\ 0 & \frac{1}{\lambda} & 0 \\ 0 & 0 & \frac{1}{\lambda} \end{bmatrix} \tag{25}$$

Since $\sigma_{22} = \sigma_{33} = 0$ and $\sigma_{ij} = 0$ for $i \neq j$, the only component of stress remaining is σ_{11}. Letting $\sigma_{11} = \sigma^{(e)}$, the constitutive equation (20) for this deformation reduces to

$$\sigma^{(e)} = 2(\lambda^2 - \frac{1}{\lambda})(\frac{\partial W}{\partial I_1} + \frac{1}{\lambda}\frac{\partial W}{\partial I_2}) \tag{26}$$

The form of W is to be determined empirically.

Forms of the Strain Energy Function

Before equation (26) can be used a suitable form of the strain energy function must be found. In determining the form of the function, the mechanical properties of the material are formulated. Material symmetries impose restrictions on the form of W which, in general, is a function of the three principal extension ratios, λ_1, λ_2, and λ_3. Isotropy restricts the form of W to symmetrical functions of the principal extension ratios. Thus W may be expressed as a function of the three strain invariants given by equation (24). The condition of incompressibility restricts W to a function of I_1 and I_2 only.

A majority of the previous theories in finite elasticity

assumes that the most general form of W for an incompressible, isotropic, elastic material is

$$W = \sum_{i=0,j=0}^{\infty} C_{ij}(I_1-3)^i\ (I_2-3)^j \qquad (27)$$

with $C_{00} = 0$ at zero strain. The simplest form of equation (27) is the strain energy function for the neo-Hookean material,

$$W = C_{10}(I_1-3) \qquad (28)$$

For small strains the constant C_{10} reduces to E/6, where E is Young's modulus, and Hooke's law is recovered. The Mooney material has a strain energy function which is dependent on I_2:

$$W = C_{10}(I_1-3) + C_{01}(I_2-3) \qquad (29)$$

Similarly, for small strains, $C_{10} + C_{01} = E/6$ giving Hooke's law.

These two simple forms of W are proposed as approximations to the strain energy function of the material under investigation. More complex forms use additional terms from equation (27) but the complexity of the resulting constitutive equation is increased. A common problem with the proposed strain energy functions is the lack of generality of the constitutive equations. Many strain energy functions yield constitutive equations that give good correlation with experimental data for a limited range of deformation or a limited number of types of deformation.

Of the more complex forms of W proposed in the past, one of the more promising and simpler versions is that suggested by Rivlin and Saunders [11]:

$$W = C_1(I_1-3) + f(I_2-3) \tag{30}$$

where the function f is to be determined empirically. This form is obviously a generalization of equations (28) and (29) but more restrictive than equation (27). Another form is that proposed by Ogden [9]. Finding equation (27) too restrictive, Ogden begins with the more general form:

$$W = W(\lambda_1,\lambda_2,\lambda_3) \tag{31}$$

and then forms the new strain invariants,

$$J(\alpha) = (\lambda_1{}^{\alpha}+\lambda_2{}^{\alpha}+\lambda_3{}^{\alpha}-3)/\alpha \tag{32}$$

where α is a real number. These invariants are related to I_1 and I_2 by

$$J(2) = \frac{1}{2}(I_1-3)$$

and $$J(-2) = -\frac{1}{2}(I_2-3) \tag{33}$$

Ogden proposes a strain energy function which is a linear combination

of these new strain invariants:

$$W = C_r J(\alpha_r) \ , \tag{34}$$

where C_r are constants related to the classical shear modulus, μ, and Young's modulus, E, by

$$C_r \alpha_r = 2\mu = \frac{2E}{3} \tag{35}$$

The Viscous Component of Stress

The viscous component of stress, represented by a dashpot, is a dissipative component which in general is a function of the deformation and the rate of deformation:

$$\underset{\sim}{\sigma}^{(v)} = - p\underset{\sim}{I} + \underset{\sim}{g}(\underset{\sim}{B},\underset{\sim}{d}) \tag{36}$$

where $\underset{\sim}{d}$ is the rate of deformation tensor. Expanding

$$\underset{\sim}{g}(\underset{\sim}{B},\underset{\sim}{d}) = K_0\underset{\sim}{I} + K_1\underset{\sim}{B} + K_2\underset{\sim}{B}^2 + K_3\underset{\sim}{d} + K_4\underset{\sim}{d}^2$$

$$+ K_5(\underset{\sim}{B}\underset{\sim}{d}+\underset{\sim}{d}\underset{\sim}{B}) + K_6(\underset{\sim}{B}^2\underset{\sim}{d}+\underset{\sim}{d}\underset{\sim}{B}^2)$$

$$+ K_7(\underset{\sim}{B}\underset{\sim}{d}^2+\underset{\sim}{d}^2\underset{\sim}{B}) + K_8(\underset{\sim}{B}^2\underset{\sim}{d}^2+\underset{\sim}{d}^2\underset{\sim}{B}^2) \tag{37}$$

where K_i(I=1,2,3,...8) are polynomials in the joint invariants of $\underset{\sim}{B}$

and $\underset{\sim}{d}$. Assuming that the viscous stress is a function of $\underset{\sim}{d}$ only, equation (36) becomes

$$\underset{\sim}{\sigma}^{(v)} = - p\underset{\sim}{I} + \underset{\sim}{k}(\underset{\sim}{d}) \tag{38}$$

with $\underset{\sim}{k}(\underset{\sim}{0}) = \underset{\sim}{0}$. Again from the assumption of isotropy, $\underset{\sim}{k}(\underset{\sim}{d})$ is an isotropic tensor function of $\underset{\sim}{d}$ and thus may be written

$$\underset{\sim}{k} = \gamma_0\underset{\sim}{I} + \gamma_1\underset{\sim}{d} + \gamma_2\underset{\sim}{d}^2 \tag{39}$$

where γ_0, γ_1, and γ_2 are scalar functions of the invariants of $\underset{\sim}{d}$ and $\gamma_0 = 0$ if the invariants of $\underset{\sim}{d}$ are zero. Then

$$\underset{\sim}{\sigma}^{(v)} = - p\underset{\sim}{I} + \gamma_0\underset{\sim}{I} + \gamma_1\underset{\sim}{d} + \gamma_2\underset{\sim}{d}^2 \tag{40}$$

which is the constitutive equation for a Reiner-Rivlin fluid. Equation (40) reduces, for a linear viscous fluid to

$$\underset{\sim}{\sigma}^{(v)} = - p\underset{\sim}{I} + \xi \operatorname{tr} \underset{\sim}{d}\ \underset{\sim}{I} + 2\eta\underset{\sim}{d} \tag{41}$$

where ξ and η are constants which are independent of $\underset{\sim}{d}$. If the fluid is also incompressible, $\operatorname{tr} \underset{\sim}{d} = 0$, and thus

$$\underset{\sim}{\sigma}^{(v)} = - p\underset{\sim}{I} + 2\eta\underset{\sim}{d}\ , \tag{42}$$

η is the viscosity coefficient. In Cartesian tensor notation,

equation (40) may be written:

$$\sigma_{ij}^{(v)} = (\gamma_0 - p)\delta_{ij} + \gamma_1 d_{ij} + \gamma_2 d_{ik} d_{kj} \tag{43}$$

In the case of simple uniaxial compression

$$d_{11} = \frac{\dot{\ell}}{\ell} = \frac{\dot{\lambda}}{\lambda} \tag{44}$$

The condition of incompressibility gives

$$d_{ii} = 0 \ , \tag{45}$$

from which it follows that

$$d_{22} + d_{33} = - \frac{\dot{\lambda}}{\lambda} \tag{46}$$

Since $\sigma_{22}^{(v)} = \sigma_{33}^{(v)} = 0$; $d_{22} = d_{33} = - \dot{\lambda}/2\lambda$, the remaining viscous stress component, $\sigma_{11}^{(v)} = \sigma^{(v)}$, in an incompressible linear viscous fluid under uniaxial compression is

$$\sigma^{(v)} = 3\eta \frac{\dot{\lambda}}{\lambda} \tag{47}$$

The viscosity coefficient, η, is to be determined empirically.

The Nonlinear Kelvin-Voigt Solid

The basic element of the Kelvin-Voigt model consists of a spring in parallel with a dashpot. In the linear theory both components are linear. A nonlinear model results when one of the components is nonlinear.

The response of the linear spring to a force F is

$$F = kx \tag{48}$$

where k is the spring modulus and x is the extension. Similarly, the response of the linear dashpot is governed by

$$F = \eta\dot{x} \tag{49}$$

where η is the viscosity.

In this investigation a creep test is used to determine the viscoelastic response of the material. A load is applied, held constant, and the deformation is recorded as a function of time. The response of a linear Kelvin-Voigt model is governed by the differential equation

$$kx + \eta\dot{x} = CH(t) \tag{50}$$

where x, the deformation, is a function of time, C is a constant, and H(t) is the Heaviside unit step function.

From the initial condition x = 0 at t = 0, the solution of equation (50) is

$$x(t) = \frac{C}{k} \{1 - \exp(-\frac{k}{\eta} t)\} H(t) \tag{51}$$

The generalized Voigt model consists of Kelvin-Voigt elements in series with a Maxwell element, which is a spring in series with a dashpot. The response is

$$x(t) = C(\frac{1}{k_m} + \frac{1}{\eta_m} t) H(t) + C \sum_{i=1}^{n} \{1 - \exp(-\frac{k_i}{\eta_i} t)\} H(t) \tag{52}$$

where k_m and η_m are the constants of the Maxwell element and n is the number of Kelvin-Voigt elements. The first term, representing the response of the Maxwell element, allows for instantaneous elasticity.

For the nonlinear Kelvin-Voigt model it is assumed that the total stress is the sum of the elastic component of stress and the viscous component of stress:

$$\underset{\sim}{\sigma} = \underset{\sim}{\sigma}^{(e)} + \underset{\sim}{\sigma}^{(v)} \tag{53}$$

Thus combining equations (14) and (40) gives

$$\underset{\sim}{\sigma} = \psi_0 \underset{\sim}{I} + \psi_1 \underset{\sim}{B} + \psi_2 \underset{\sim}{B}^2 - p\underset{\sim}{I} + \gamma_0 \underset{\sim}{I} + \gamma_1 \underset{\sim}{d} + \gamma_2 \underset{\sim}{d}^2 \tag{54}$$

The assumption of incompressibility reduces this to

$$\underset{\sim}{\sigma} = - p\underset{\sim}{I} + \psi_1 \underset{\sim}{B} + \psi_2 \underset{\sim}{B}^2 + \gamma_1 \underset{\sim}{d} + \gamma_2 \underset{\sim}{d}^2 \tag{55}$$

which is the constitutive equation for an isotropic incompressible Kelvin-Voigt solid.

The simplest nonlinear Kelvin-Voigt model is one where the spring is nonlinear and the dashpot is linear. Then for the case of uniaxial compression, equations (26) and (47) give

$$\sigma = 2(\lambda^2 - \frac{1}{\lambda})(\frac{\partial W}{\partial I_1} + \frac{1}{\lambda}\frac{\partial W}{\partial I_2}) + 3\eta\frac{\dot{\lambda}}{\lambda} \tag{56}$$

Further reduction is obtained if a neo-Hookean material is assumed for the nonlinear spring:

$$\sigma = 2C_1(\lambda^2 - \frac{1}{\lambda}) + 3\eta\frac{\dot{\lambda}}{\lambda} \tag{57}$$

Now if a step load, CH(t), is applied, equation (57) may be written

$$\frac{CH(t)}{A} = 2C_1(\lambda^2 - \frac{1}{\lambda}) + 3\eta\frac{\dot{\lambda}}{\lambda} \tag{58}$$

where $A = A_0/\lambda$ is the current cross-sectional area of the sample. Letting $K = CH(t)/2A_0C_1$, the variables can be separated in equation (58), yielding

$$\frac{d\lambda}{\lambda^3 - K\lambda^2 - 1} = -\frac{2C_1}{3\eta}dt \tag{59}$$

In general, the cubic polynomial, $\lambda^3 - K\lambda^2 - 1$ may be separated into $(\lambda-R)(\lambda^2+P\lambda+Q)$, where R is the real root of the polynomial. Equation

(59) is then integrable and the solution is a transcendental equation having the form

$$t = -\frac{3\eta}{4C_1(Q+RP+R^2)}\left[\ln\frac{(\lambda-R)^2}{(\lambda^2+P\lambda+Q)} - \frac{2(2R+P)}{\sqrt{(4Q-P^2)}}\tan^{-1}\frac{2\lambda+P}{\sqrt{(4Q-P^2)}}\right] + S \quad (60)$$

where S, the constant of integration, is

$$S = \frac{3\eta}{4C_1(Q-RP+R^2)}\left[\ln\frac{(1+R)^2}{(1+P+Q)} - \frac{2(2R+P)}{\sqrt{(4Q-P^2)}}\tan^{-1}\frac{2+P}{\sqrt{(4Q-P^2)}}\right] \quad (61)$$

This equation is used as a first approximation to the viscoelastic behavior of the polyurethane material. Inspection of equations (56) to (59) shows that numerical methods are required for more complex forms of W and if $\eta = \eta(\lambda)$.

If the Mooney form of W is chosen for the spring, the constitutive equation for the elastic part becomes

$$\sigma^{(e)} = 2(\lambda^2 - \frac{1}{\lambda})(C_1 + \frac{C_2}{\lambda}) \ . \quad (62)$$

Numerical integration is required to solve the resulting differential equation. The form suggested by Ogden [9] yields

$$\sigma^{(e)} = C_r(\lambda^{\alpha_r} - \lambda^{-\alpha_r/2}) \ , \quad (63)$$

and when combined with the viscous tensor also requires numerical integration, unless $r = 1$ and $\alpha_1 = 2$ in which case the neo-Hookean form

is recovered. Similarly, the form suggested by Rivlin and Saunders [11] in its simplest variation gives the same result as the Mooney form and other variations give rise to complex nonlinear differential equations.

CHAPTER III

EXPERIMENTAL INVESTIGATION

Description of Apparatus

The apparatus consists of two separate systems: the environmental control system and the compression testing system. Basically, the environmental control system is a refrigeration system which is capable of lowering a sample from room temperature (70°F) to 0°F and maintaining a set temperature within a tolerance of $\pm$ 2°F. The compression testing system consists of a subpress and a testing machine. A schematic drawing of the apparatus is shown in Figure 3.

The refrigeration system, except for the evaporator coil, is supplied by a commercial refrigeration manufacturing firm. It consists of a single stage 1/3 horsepower reciprocating compressor, a water-cooled condenser, a drier, a solenoid valve, a thermostatic expansion valve, and a thermostat control. The compressor is air cooled by a fan. A solenoid valve is placed upstream of the expansion valve to minimize "overshooting" of the desired temperature. This valve closes when the compressor shuts off and prevents refrigerant from passing through the evaporator. A 2-1/2°F temperature differential thermostat is used to control the compressor. The sensor is placed on the subpress block to take advantage of its thermal inertia and the fact that its temperature variation approximates that of the test specimen in the platens. The refrigerant is

KEY:

1 Compressor
2 Condensor
3 Drier
4 Solenoid Valve
5 Expansion Valve
6 Subpress Block
7 Compression Cylinder
8 Evaporator Coil
9 Light
10 Upper Platen
11 Sample
12 Lower Platen
13 Thermostat Sensor
14 Metal Inserts
15 Access Window
16 Lower Compression Head
17 Upper Compression Head
18 Polyethylene Shroud
19 Thermostat

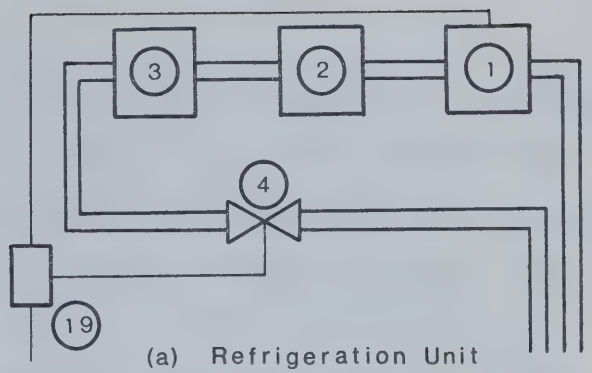

(a) Refrigeration Unit

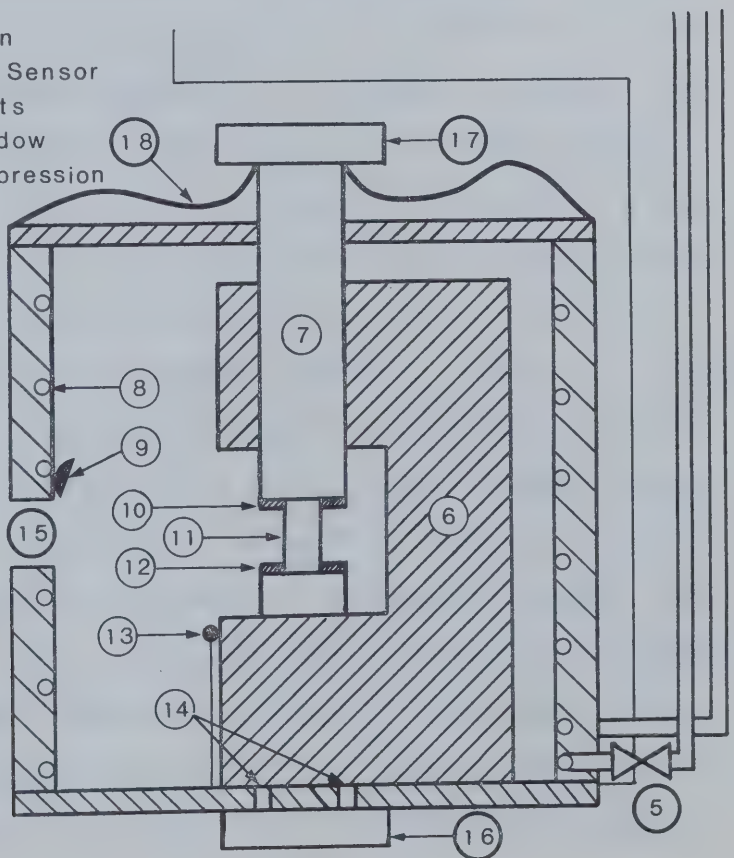

(b) Environmental Chamber

FIGURE 3 APPARATUS

freon 12.

The evaporator coil of the refrigeration system is the cooling coil of the environmental chamber. This chamber consists of two concentric cylinders of galvanized iron with the cooling coil soldered to the inner cylinder in the wall space between the cylinder. Heat transfer from inside the chamber is thus improved and styrofoam insulation is used to reduce transfer from the outer shell. The base of the chamber is a 3/4 inch thick wooden plate with four 1/8 inch diameter steel inserts embedded in it to support the subpress. The top, also a 3/4 inch thick wooden plate, has a circular opening in it to accommodate the compression cylinder of the subpress. A polyethylene shroud covers the exposed shaft of the compression cylinder and the opening to prevent the formation of ice on the shaft which renders it immovable at temperature below 32°F. Access to the inside of the chamber is made through a doorway in the mid-section of the cylinder and a plexiglass door is fitted to allow viewing. Inside, the subpress is attached by fins to two rings, which are in contact with the inner wall of the chamber, for greater heat transfer. With this arrangement, it is possible to maintain the subpress temperature, and thus the sample temperature, within $\pm$ 2°F of the desired temperature. Below the access doorway is a shelf which provides storage space for the specimen. A small light is placed above the doorway for illumination.

The subpress component of the testing apparatus is a Tinius Olsen model which has been modified for these particular testing conditions. Modifications include the revision of the lower platen,

which was free to swivel, to make it rigid and parallel to the top platen; the addition of fins to provide a more efficient heat transfer path. The testing machine used is made by Gilmore Industries. It has a 50,000 pound capacity hydraulic fatigue test frame with a modular electronic control panel. The compression piston has a maximum travel of 6 inches. For the tests the lowest load range (0 - 5000 pounds) is used. The load to the nearest ten pounds and the displacement to the nearest thousandth of an inch are read directly from a digital voltmeter in the control panel.

Miscellaneous equipment include a potentiometer, a switching box, a strip chart recorder, and a micrometer. Copper constantan thermocouples with an ice bath as the reference junction are used to measure the temperature. A thermocouple is embedded in a sample which is placed between the platens of the subpress. Then under test conditions, a position is found on the subpress block where the temperature and its variation closely resembled that of the test specimen. The sample with the embedded thermocouple is left on the shelf to indicate the temperature of samples sitting on the shelf. Another thermocouple is attached to the subpress block at the position located by the trial and error procedure mentioned above to indicate the temperature of a sample in the subpress. These thermocouples are connected to a switching box which is connected to the potentiometer or the strip chart recorder. A micrometer, which is accurate to the nearest thousandth of an inch, is used to measure the dimensions of the samples.

The design specifications of the environmental chamber and subpress modification are given in Sheriff [12].

Preparation of Samples

The polyurethane material presents some difficulties in the preparation of test samples. A commercial manufacturer provides the material in 3/4 inch diameter rods which are 3-1/2 inches long. These rods are cut into 3/4 inch and 1 inch lengths on a lathe using a spring collett chuck. A coolant is used in the cutting operation to prevent excessive temperature rise in the sample. This gives a reasonable finish as well as parallel ends. To achieve as smooth a finish as possible, the ends are polished by successively finer grades of abrasive paper on a belt grinder. A Surfmet grinder, model 16-1255, made by Buehler Ltd., fitted with Speed Wet Durite Cloth belts is used with water as a coolant. Final polishing is done by hand on very fine abrasive paper.

Experimental Procedure

The polished ends of a sample are lubricated with a silicone lubricant and the sample is placed between the compression platens of the subpress. The compression heads of the testing frame are applied to the subpress compression piston but with zero load. The chamber, subpress and sample are allowed to reach the desired test temperature. Then the sample is removed and a micrometer is used to obtain initial dimensions of the sample at test conditions. Centering the sample in the subpress platens again, the sample is allowed to reach equilibrium before applying a load. The first load increment is applied and held until the deformation reaches a steady constant value, which is recorded with the load and the temperature. Also the

time required for the deformation to reach its equilibrium value is recorded. These steps are repeated for further increments of load. After the final load increment has been applied, the sample is unloaded completely, measured, and then allowed to recover in the chamber at the test temperature. By making measurements of the sample length at regular intervals, a recovery curve may be obtained. The equilibrium load-deformation data give the stress-strain curve and thus shows the static elastic response of the material.

To determine the viscous response a creep test is performed. A step load is applied and held on the specimen and the resulting deformation is recorded at regular time intervals. This test gives a creep curve for the material at the test temperature and repetition of the test at other temperatures gives the effect of temperature on the viscous response.

Analysis of Data

The static elastic response data, obtained by allowing the deformation to reach equilibrium, are shown in Figure 4 in the form of stress versus extension ratio curves. Four different temperature tests are shown indicating the effect of temperature on the elastic response of the material. Also plotted on this figure are the various responses predicted by the theoretical models. The neo-Hookean and Mooney predictions are inadequate for $\lambda < 0.95$. A single term version of Ogden's suggested strain energy function is also inadequate in predicting the material's static elastic response.

Since the simple theoretical models are inadequate, a new model based on the Rivlin-Saunders form of the strain energy function

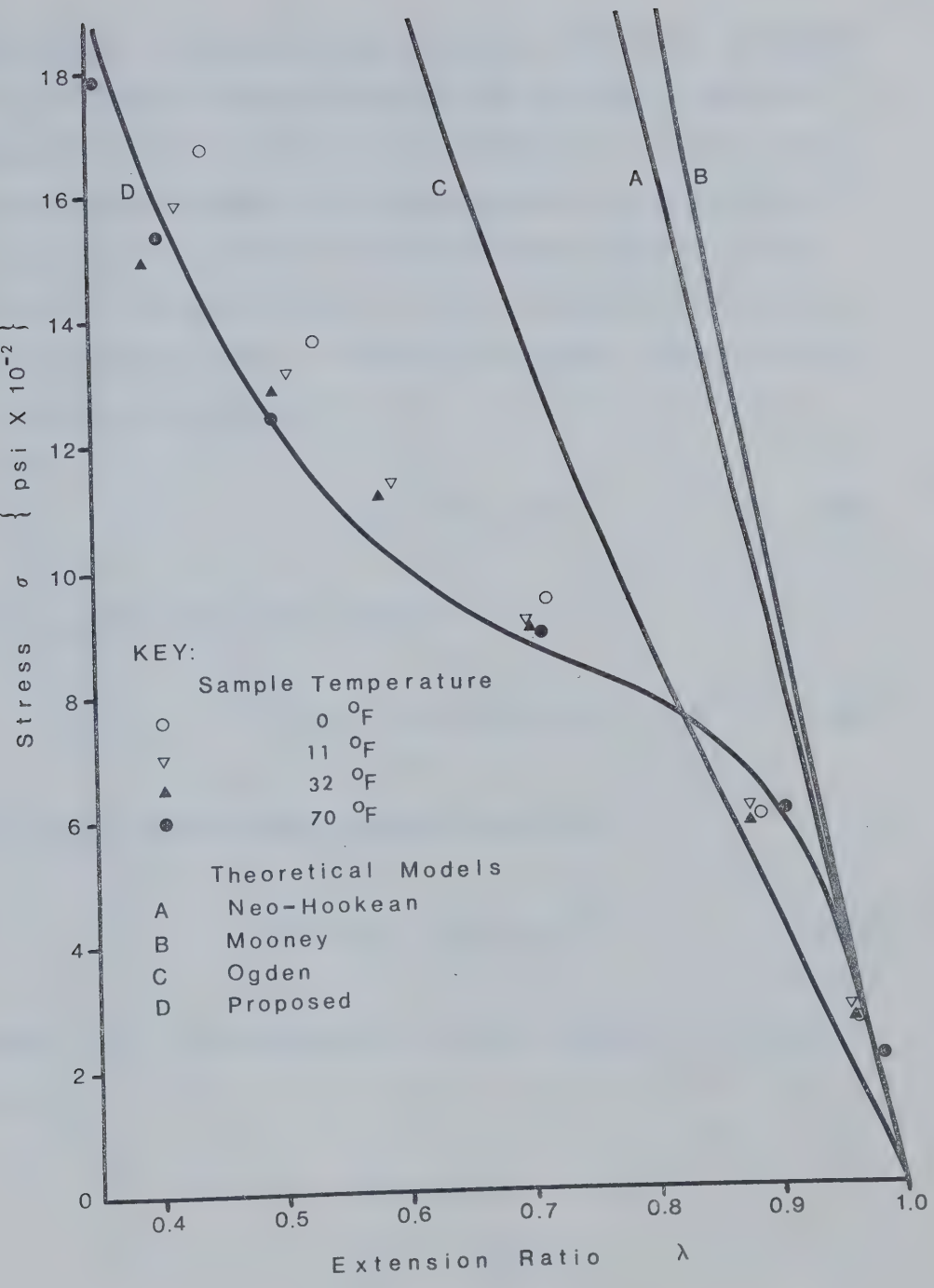

FIGURE 4 ELASTIC RESPONSE CURVES

is proposed. It is assumed that the stress-strain curve is composed of two elementary curves arising from the two terms of the strain energy function. The first term of equation (30) by itself results in the neo-Hookean model. By an appropriate choice of C_1 the neo-Hookean model correlates with the experimental data for $\lambda < 0.5$. Then to fit the data for $0.5 < \lambda < 1.0$, the second curve must have the form $K(1-\lambda^{\alpha})$, where $\alpha > 1$ and K is a constant. Thus the form of f required in equation (30) is

$$f(I_2) = \lambda^{\alpha} I_2 - 3 \tag{64}$$

The proposed strain energy function is

$$W = C_1(I_1-3) + C_2(\lambda^{\alpha} I_2-3) \tag{65}$$

which gives the following constitutive equation:

$$\sigma^{(e)} = 2(\lambda^2 - \frac{1}{\lambda})(C_1+C_2\lambda^{\gamma}) \tag{66}$$

where $\gamma > 0$. The constants which provide a reasonable fit to the data are

$$C_1 = 350 \text{ psi}$$

$$C_2 = -1420 \text{ psi}$$

$$\gamma = 7$$

and this is curve D in Figure 4. Curve D follows the deformation of the room temperature sample very closely. To fit the cooler temperature data, a smaller value of γ is required.

In Figure 4 curve A represents the neo-Hookean prediction with C_1 = 1400 psi. Curve B is the Mooney representation using C_1 = 1400 psi and C_2 = 1272 psi. Curve C is a single term version of Ogden's strain energy function with C_1 = 750 psi and α_1 = 4.

The viscoelastic response of the material is shown in Figure 5. The data shown represent the most consistent results obtrained in the creep tests. Using the equilibrium value of the deformation from these results, appropriate values of the constants C_1 and η in equation (60) are obtained. Also, the root R is the equilibrium value of the deformation. Thus with R = 0.958, C_1 = 800 psi and η = 2000 lb-sec/in^2 equation (60) is plotted in Figure 5 for comparison.

Since the samples are not measured at the exact test temperature a correction for thermal expansion may be required. Figure 6 shows the effect of temperature on the length of the sample. The maximum change in length is 0.01 inch for a temperature differential of 70°F. Thus the coefficient of thermal expansion for this material is 0.000143 in/°F. In removing the sample from the environmental chamber, the sample temperature rises as much as 10°F before the measurement is made. Thus the difference between the measured length of a sample and its actual length at the test temperature is less than 0.001 inch. This difference is assumed to be negligible since the resolution of the micrometer is only 0.001 inch.

Figure 7 shows the effect of the sample size on the response. The shorter samples appear to be slightly stiffer than the longer

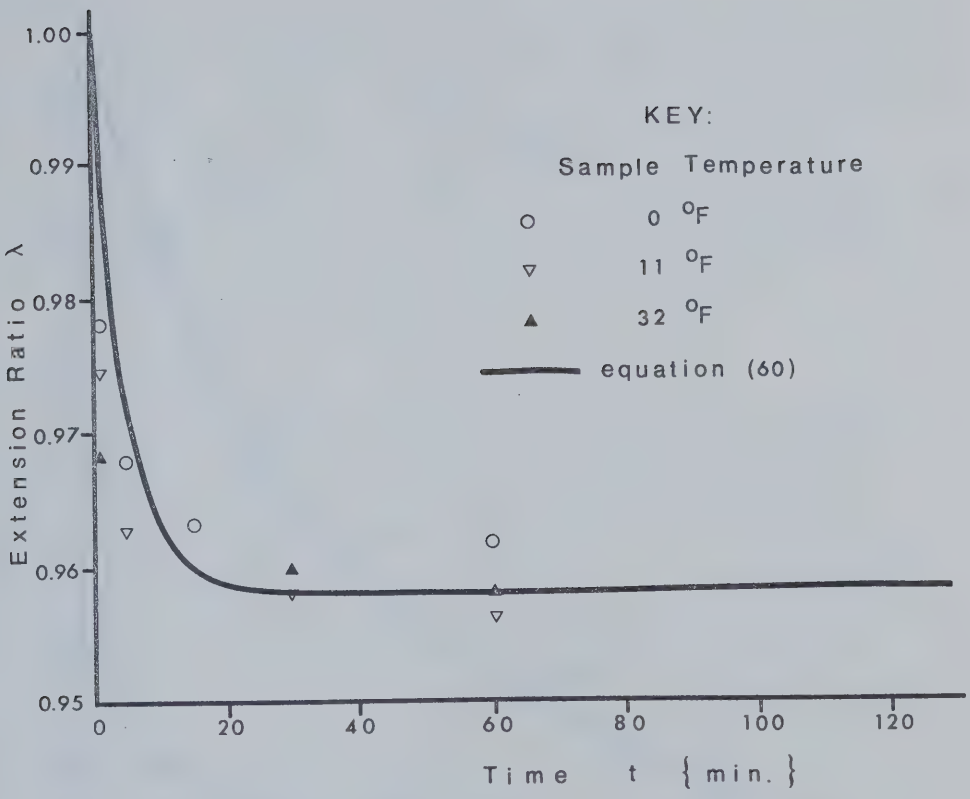

FIGURE 5 VISCOUS RESPONSE CURVES

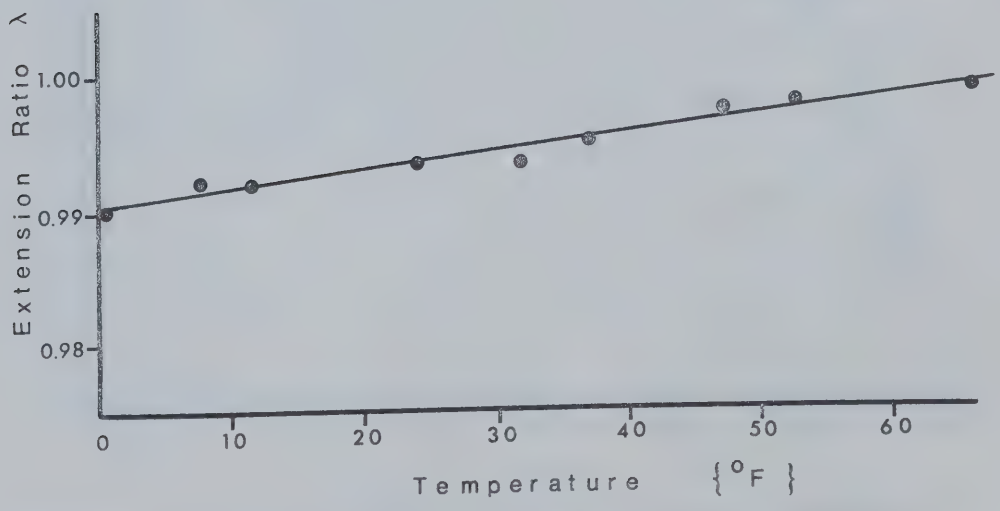

FIGURE 6 THERMAL EXPANSION OF POLYURETHANE

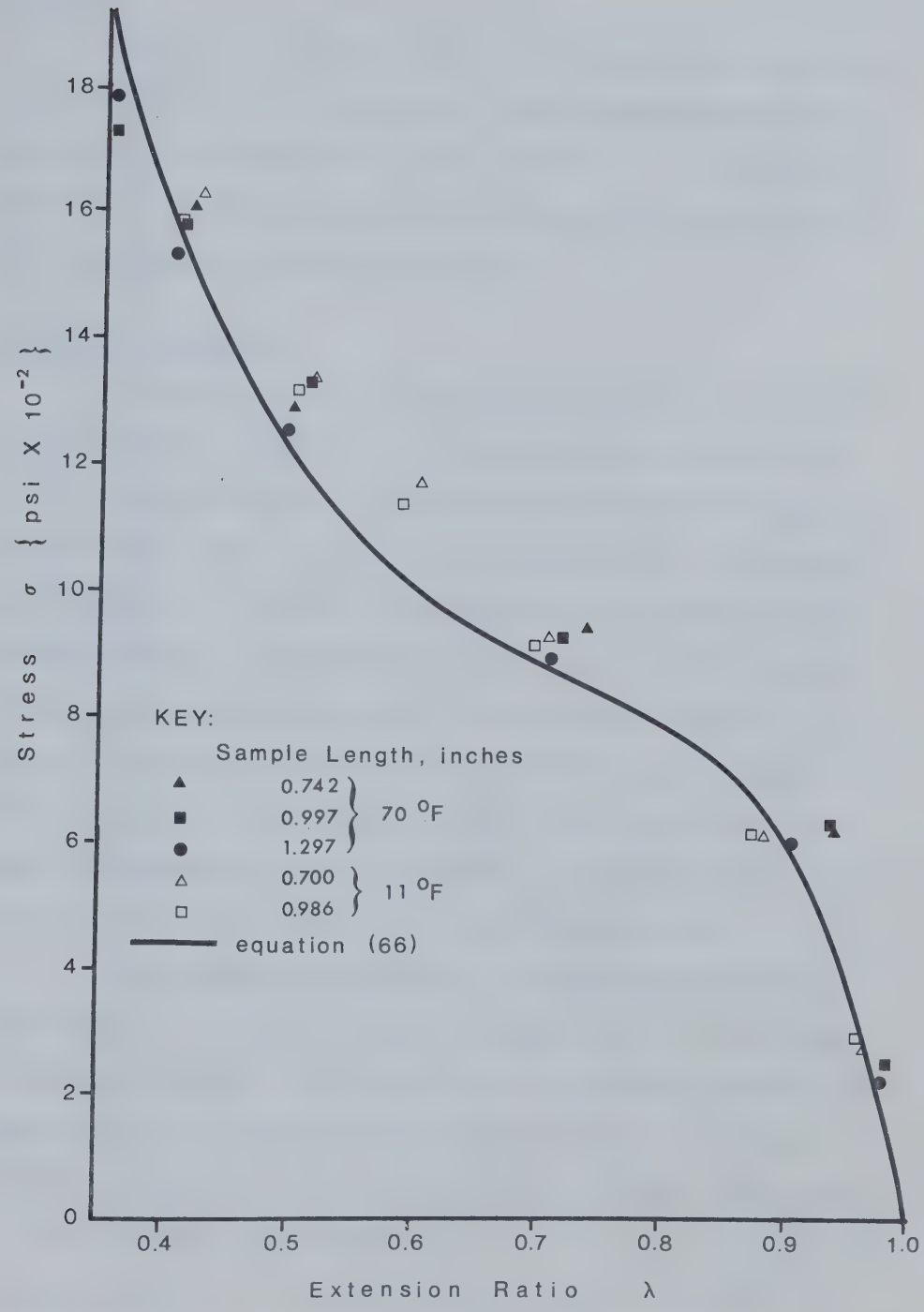

FIGURE 7 EFFECT OF SAMPLE SIZE ON THE ELASTIC RESPONSE

samples.

The use of a subpress may require a correction for the subpress deformation. For the range of loads used the deformation of the subpress is elastic and is shown in Figure 8. The maximum deformation is 0.003 inch which is insignificant when compared to a sample deformation of more than 0.5 inch.

Discussion of Results

The static elastic response of the polyurethane material shown in Figure 4 appears to differ from the tension results obtained with other rubber-like materials by previous investigators. Earlier results show a continuously increasing slope to the stress-strain curve as λ increases. The present investigation of a polyurethane material in compression indicates that an inflection point exists in the stress-strain curve. As λ decreases from 1.0, the slope of the stress-strain curve decreases until the inflection point is reached. Experiments performed in equi-biaxial tension, which is equivalent to simple compression, by previous investigators also show this slope characteristic and inflection point.

While previous investigators had some success in using simple models to predict the elastic response, this is not the case in this investigation. All three of the simple models attempted are inadequate in predicting the response characteristics of the polyurethane. The models can predict the response at small deformations ($\lambda > 0.95$) and very large deformation ($\lambda < 0.5$), but do not show an inflection point or the transition zone of moderate strains. The proposed model does predict the response curve but it lacks the

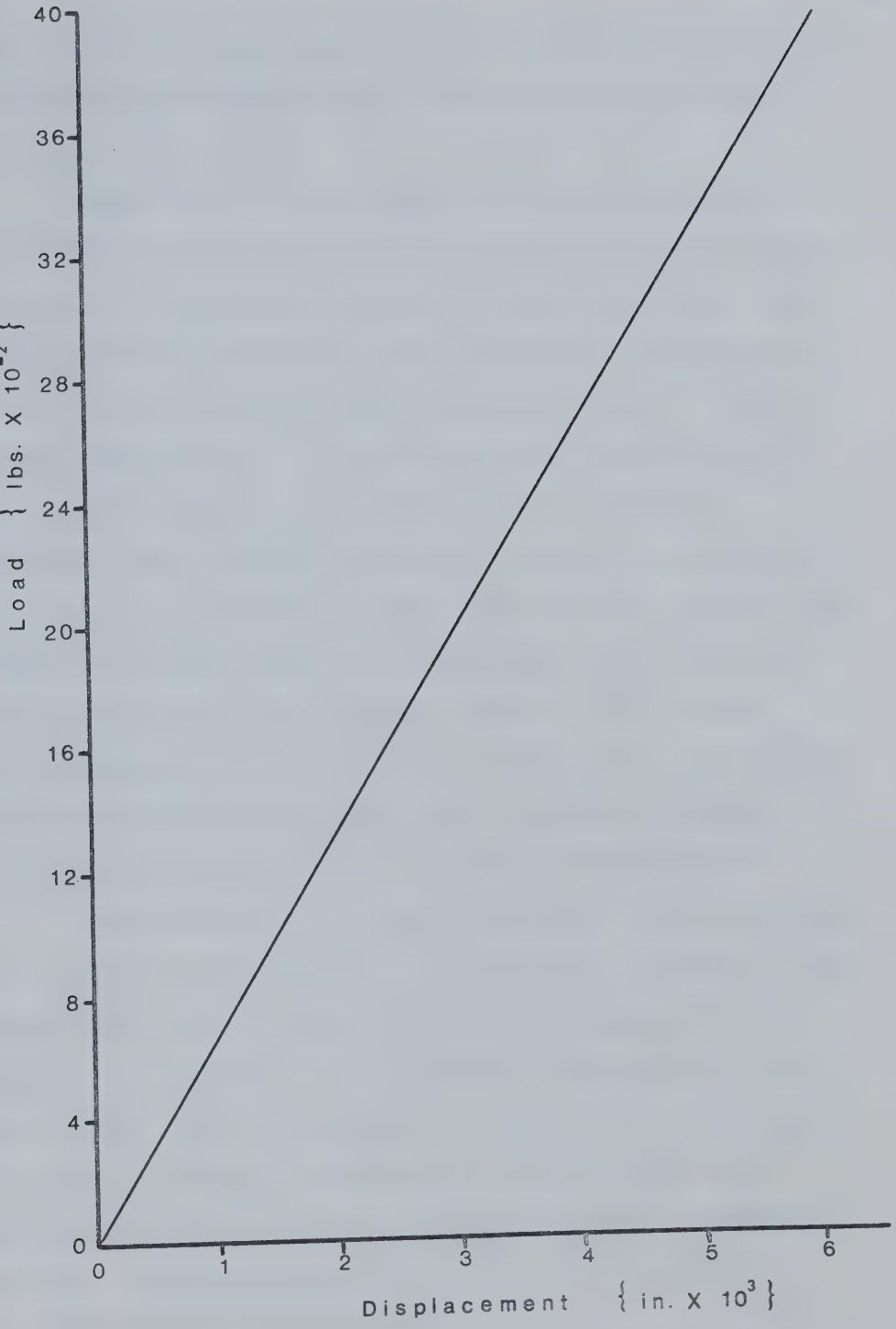

FIGURE 8 SUBPRESS DEFORMATION

generality of the simpler models. It is valid for uniaxial compression only and the strain energy function used in its derivation does not meet symmetry restrictions.

Comparison of curve D with the experimental data reveals a very good correlation between the proposed model and the room temperature data. The response data obtained at cooler temperatures show a stiffening effect in that these curves are flatter. One explanation of this behavior is that the material exhibits a change in behavior at cooler temperatures. This explanation appears to be reasonable since a gradual change in the response curve is observed with the temperature change. However, the change is primarily at large deformation and at small deformations there appears to be no change in the response curve with a change in the temperature. Also barrelling of the sample occurs for fairly moderate strains ($\lambda < 0.9$) and the error introduced by this barrelling is not known. Thus it is possible that the difference in the response data is caused by a change in the performance of the lubricant at the different temperatures.

The lubricant is a silicone release agent. Other lubricants tried include machine oil, grease, petroleum jelly, graphite oil, and calcium oleate. With the exception of calcium oleate, all these lubricants are squeezed out upon application of some load and the sample barrels. Barrelling occurs even with calcium oleate but it occurs at larger loads. The problem with calcium oleate is the difficulty in application and its significant amount of deformation under load. The silicone lubricant gives the best compromise of lubrication qualities with convenience.

The results of the creep tests are inconclusive since the scatter in the data obtained is excessive. Except for the data presented in Figure 5, no definite trends are observable in the creep data. One reason for the poor data is the inaccurate step loading technique required by the testing machine. Since there is no provision for a perfect step function, such a load is applied by presetting the required step electronically and then switching on the hydraulics to execute this loading. The resulting load function is inconsistent, varying with each preset load, and inaccurate (overshooting the preset load). Other reasons include the lubrication problem and the temperature effect.

The viscoelastic model presented in Figure 5 is based on a neo-Hookean spring in parallel with a linear viscous dashpot. Poor correlation with data is probably due to the assumption of a neo-Hookean spring which proved inadequate in the static elastic case. The use of a more complex nonlinear spring results in a differential equation which requires numerical methods to solve. Since the data is poor more complex models are not attempted at this time.

Because of the unknown errors involved in this investigation a quantitative error analysis is not made here. Some of the sources of errors include the digital voltmeter in the control panel of the testing machine, the load control, the micrometer, the thermostat, and the thermocouples. The digital meter has a load resolution of 10 pounds and a displacement resolution of 0.001 inch. The load control is capable of maintaining a preset load to a tolerance of $\pm$ 10 pounds. This results in a displacement accuracy of $\pm$ 0.001 inch. The micrometer has a resoltuion of 0.001 inch. The thermostat

differential is 2.5°F and the resolution of the thermocouples is ± 1°F. Of the unknown errors, the most important is probably the effect of barrelling. Another is the previous history of the samples. Since the samples are supplied by a commercial firm, their history is not known exactly. Some samples appear to have more entrapped bubbles than others. Despite these unknowns the results obtained for the static case are consistent.

Informal recovery data indicate that over 90% of the original length is recovered within the first ten hours after unloading. Eventually samples which were loaded to 1200 pounds recover 99% to 100% of their original length; those loaded to 1800 pounds recover 93% of their original length. This indicates that permanent set occurs in this material for some load between 1200 and 1800 pounds.

Appendix A contains the data for the elastic response curves. The data for the viscous response curves are contained in Appendix B. The recovery data are given in Appendix C. Calibration data for the Gilmore testing machine are in Appendix D. Finally, Appendix E contains a list of the materials and equipment used.

CHAPTER IV

CONCLUSIONS

The static elastic response and the viscoelastic response of a polyurethane material under compression are studied in this thesis. For the elastic response the simple models are shown to be inadequate for compression deformation. A new model is proposed which correlates with the data but lacks generality. The viscoelastic response data are relatively inconclusive, but they do indicate that a more complex version of the nonlinear Kelvin-Voigt model is required. This conclusion agrees with the results of the elastic response tests.

In the range of temperatures studied, the temperature does not appear to have a significant effect on the elastic response of the material. This is especially true at small deformations. At large deformations a stiffening effect is observed with cooler temperature.

Thus these compression tests indicate a behavior that differs from that observed by previous investigation using tension tests. To confirm this, it is recommended that a tension test be performed on this material.

BIBLIOGRAPHY

1. ADKINS, J.E., "Large Elastic Deformations", Progress in Solid Mechanics, Vol. 2, edited by I.N. Sneddon and R. Hill, North Holland Publishing Co., Amsterdam, 1961.
2. ALEXANDER, H., "A Constitutive Relation for Rubber-Like Materials", Int. J. Engng. Sci., Vol. 6, Pergamon Press, 1968, p. 549.
3. BLAND, D.R., The Theory of Linear Viscoelasticity, Pergamon Press, Oxford, 1960.
4. ERINGEN, A.C., Mechanics of Continua, John Wiley & Sons, New York, 1967.
5. GREEN, A.E., and J.E. ADKINS, Large Elastic Deformations and Non-linear Continuum Mechanics, Oxford University Press, London, 1960.
6. GREEN, A.E., and W. ZERNA, Theoretical Elasticity, Oxford University Press, London, 1954.
7. LEIGH, D.C., Nonlinear Continuum Mechanics, McGraw-Hill Book Co., New York, 1968.
8. MALVERN, L.E., Introduction to the Mechanics of a Continuous Medium, Prentice-Hall, Englewood Cliffs, N.J. 1969.
9. OGDEN, R.W., "Large Deformation Isotropic Elasticity", Proc. R. Soc. London, A326 (1972), p.565.
10. PEARSON, C.E., Theoretical Elasticity, Harvard University Press, Cambridge, Mass., 1959.

11. RIVLIN, R.S., and D.W. SAUNDERS, "Large Elastic Deformations of Isotropic Materials VII. Experiments on the Deformation of Rubber", Phil. Trans. Roy. Soc. of London, Series A, Vol. 243, 1950-51, p. 251.

12. SHERIFF, J., "Low Temperature Compression Test Apparatus", M.Eng. Thesis, University of Alberta, Edmonton, 1972.

13. SPENCER, A.J.M., "The Static Theory of Finite Elasticity", J. Inst. Maths. Applics. (1970) 6, p. 164.

14. TRELOAR, L.R.G., The Physics of Rubber Elasticity, Oxford University Press, London, 1967.

APPENDIX A

ELASTIC RESPONSE DATA

Load (lb.)	Deformation of Sample $\Delta\ell$ (in.)						
	T = 0°F ℓ_o=0.991 in.	T = 11°F ℓ_o=0.986 in.	T = 11°F ℓ_o=0.700 in.	T = 32°F ℓ_o=0.988 in.	T = 70°F ℓ_o=0.742 in.	T = 70°F ℓ_o=0.997 in.	T = 70°F ℓ_o=1.297 in.
100	0.038	0.043	0.026	0.041	0.012	0.018	0.026
300	0.115	0.125	0.084	0.122	0.052	0.067	0.125
600	0.283	0.297	0.205	0.295	0.193	0.283	0.379
900	--	0.404	0.278	0.413	--	--	--
1200	0.464	0.485	0.338	0.500	0.368	0.484	0.654
1800	0.437	0.412	0.399	0.598	0.430	0.584	0.772
2400	--	--	--	--	--	0.643	0.837

APPENDIX B

VISCOUS RESPONSE DATA

Time (min.)	Deformation of Sample $\Delta\ell$ (in.)						
	Load = 100 lb.					Load = 300 lb.	
	T = 0°F ℓ_o=0.991 in.	T = 11°F ℓ_o=0.700 in.	T = 11°F ℓ_o=0.986 in.	T = 32°F ℓ_o=0.988 in.	T = 32°F ℓ_o=1.000 in.	T = 70°F ℓ_o=0.729 in.	T = 70°F ℓ_o=0.727 in.
1	0.022	0.020	0.026	0.031	0.038	0.103	0.104
5	0.032	0.025	0.036	0.036	0.044	0.109	0.111
15	0.037	0.027	0.039	0.038	0.046	0.109	0.115
30	0.038	--	0.041	0.040	0.047	0.112	0.116
60	0.038	0.026	0.043	0.041	0.047	0.119	0.117
120	--	--	--	--	--	0.124	0.119
180	--	--	--	--	--	0.126	0.120

APPENDIX C

RECOVERY DATA

Time	Sample Length, ℓ (in.)							
	L = 1200 lb. T = 0°F ℓ_o=0.742 in.	L = 1800 lb. T = 0°F ℓ_o=1.001 in.	L = 1800 lb. T = 11°F ℓ_o=0.700 in.	L = 1800 lb. T = 11°F ℓ_o=0.986 in.	L = 1800 lb. T = 32°F ℓ_o=0.988 in.	L = 1800 lb. T = 32°F ℓ_o=1.000 in.	L = 1800 lb. T = 70°F ℓ_o=0.742 in.	L = 2400 lb. T = 70°F ℓ_o=1.297 in.
0	0.698	0.442	0.301	0.412	0.390	0.349	0.311	0.460
10 hr.	0.736	0.946	0.674	0.970	0.955	0.958	0.652	1.051
24 hr.	0.740	0.976	0.689	0.971	0.963	0.971	0.691	1.195
3 days	0.742	0.980	0.692	0.976	0.965	0.978	0.700	1.225
6 days	0.742	0.997	0.692	0.978	0.970	0.982	0.705	1.227
12 days	0.742	0.997	0.697	0.981	0.974	0.985	0.709	1.230

APPENDIX D

CALIBRATION

Calibration of Load Cell

The load cell of the Gilmore testing machine is calibrated using Morehouse Proving Rings #4005 and #4006. Proving ring #4005 has a capacity of 500 lb. compression and #4006 has a capacity of 4000 lb. compression. The rings are calibrated by dead weights by National Standards Testing Laboratory. The temperature during calibration is 70°F.

CALIBRATION DATA - RING #4005

Machine Reading	Instrument Reading	Temperature Correction	Corrected Reading	Force Applied	Error	
lb.	div.	div.	div.	lb.	lb.	%
50	92.45	0.06	92.51	52.62	2.62	4.98
100	212.60	0.13	212.73	108.94	8.94	8.21
200	456.90	0.28	457.18	232.38	32.38	13.85
300	660.25	0.40	660.65	333.71	33.71	10.11
400	785.05	0.47	785.52	395.27	4.73	1.20

CALIBRATION DATA - RING #4006

Machine Reading	Instrument Reading	Temperature Correction	Corrected Reading	Force Applied	Error	
lb.	div.	div.	div.	lb.	lb.	%
400	102.30	0.06	102.36	413.9	13.9	3.37
500	125.70	0.08	125.78	509.5	9.5	1.87
600	152.00	0.10	152.10	615.7	15.7	2.55
1000	253.70	0.16	253.86	1024.5	24.5	2.39
1200	303.60	0.19	303.79	1224.4	24.4	1.99
1600	404.60	0.25	404.85	1626.8	26.8	1.65
2400	610.10	0.37	610.47	2438.9	38.9	1.60

Calibration of Displacement Transducer

A dial deflection gauge is used to check the displacement transducer. The transducer is accurate to within 0.001 inch of the dial gauge reading over the entire 6 inch travel of the compression piston. An Oldak Precision Dial Indicator, model MS38, is used.

APPENDIX E

LIST OF MATERIALS AND EQUIPMENT

Materials

Polyurethane elastomer: Vibrathane 6006 (Uniroyal Chemical)

Silicone release agent: GE SF-96A (General Electric)

Equipment

50,000 lb. test frame: model 426-50 (Gilmore Industries)

Subpress: model 85573 (Tinius Olsen Testing Machine Co.)

Millivolt potentiometer: model 8686 (Leeds and Northrup Co.)

Graphic recorder: model G-14A-1 (Varian Associates)

Switching box: model 220 (Baldwin-Lima-Hamilton Corp.)

Refrigeration unit: special model (Associated Refrigeration Industry)

Micrometer: caliper type (Moore and Wright)

Proving rings: #4005 and #4006 (Morehouse)

Dial indicator: model MS38 (Oldak)